Available online at www.sciencedirect.com
ScienceDirect
International Journal of Heat and Mass Transfer 50 (2007) 2692–2703
International Journal of HEAT and MASS TRANSFER
www.elsevier.com/locate/ijhmt

Implications of solid phase interaction mechanisms on momentum, heat and solute transport in semi-solid materials processing

Joydeep Chowdhury, Suvankar Ganguly, Suman Chakraborty *

Department of Mechanical Engineering, Indian Institute of Technology, Kharagpur-721302, India

Received 31 December 2005; received in revised form 20 September 2006
Available online 13 March 2007

Abstract

In this work, the problem of mathematical modeling of transport phenomena during semi-solid metal processing is investigated from a fundamental approach. The phenomenon of solid phase interaction is modeled by an evolution equation of an internal state variable. The formation of an interconnected network of agglomerated solid fragments at high values of solid fraction is also accounted for, leading to a more realistic prediction of momentum transport in comparison to other standard models reported in the literature. Numerical simulations are performed based on two separate momentum transport models. One of the models essentially neglects solid phase interaction mechanisms, whereas the other one incorporates the associated transport features, in order to capture the implications of solid phase agglomeration in a semi-solid slurry processing. A detailed analysis of the results reveals a profound impact of agglomeration and break-up on the transport phenomena, which need to be effectively captured.

Keywords: Semi-solid processing; Solidification; Convection; Simulation

1. Introduction

Semi-solid metal (SSM) processing has ushered new hopes in the light metal industry, with its unique energy conserving and quality assuring features. In fact, SSM processing has paved the way for almost defect-free products in automobile industry by ensuring that several common manufacturing defects like porosity, heterogeneous composition, etc. do not virtually feature in the final product. The internal structure of a material in the semi-solid state is composed of solid globular grains suspended in a liquid metal matrix. The semi-solid slurry with a non-dendritic microstructure exhibits a distinct rheological characteristic which makes the SSM processing an effective and favored route for manufacturing of defect-free near net shape products. As more and more products are brought under the horizon of SSM processing, an urgent need for a comprehensive mathematical model to simulate semi-solid slurry processing is being felt, so as to accurately predict the resultant mechanical properties and hence the reliability in performance. In this respect, there is a strong requirement to develop a generalized modeling approach for coupled momentum, heat and species transport during semi-solid slurry processing, with an underlying emphasis on capturing the intricate details of physical phenomena occurring during SSM processes, many of which are otherwise overlooked in classical mathematical models existing in the literature.

In the literature concerning materials processing, only a few attempts to model transport phenomena during semi-solid metal processing have been reported, most of which are based on volume-averaged continuum models [1]. In most instances, such models incorporate the idea of an effective viscosity in conjunction with several empirical parameters depicting relationship between shear stress and strain rate. It can be noted in this context that the

* Corresponding author.
E-mail address: suman@mech.iitkgp.ernet.in (S. Chakraborty).

0017-9310/$ - see front matter © 2007 Elsevier Ltd. All rights reserved.
doi:10.1016/j.ijheatmasstransfer.2006.11.038

Nomenclature

B	magnetic flux vector
C_p	specific heat
C	species concentration
D	species diffusion coefficient
f	mass fraction
g	volume fraction (when subscripted), gravitational acceleration vector (when not subscripted)
h	specific enthalpy
ΔH	latent enthalpy
J	current density vector
k_{eff}	effective thermal conductivity
k_{p}	partition coefficient
p	pressure
S	source term
t	time
T	temperature
u	x-component of velocity
v	y-component of velocity
x,y	coordinate variable

Greek symbols

β_{s}	solutal volumetric coefficient
β_{t}	thermal volumetric coefficient
ρ	density
μ	dynamic viscosity
μ_{eff}	effective viscosity
ϕ	general scalar variable

Subscripts

l	liquid phase
mix	mixture
ref	reference
s	solid phase

formation of a globular microstructure during SSM processing primarily accounts for the final product quality, and an intense stirring during solidification eventually leads to this special microstructure [2–6]. However, as solidification progresses, the fundamental characteristics of the stirred melt also change, especially beyond a certain critical value of solid fraction. This aspect has been emphasized by Mat and Illegbusi [7] in the development of a hybrid model to simulate the flowability of the mushy zone, with a quantitative capability to predict the final macrosegregation pattern. The above model divides the entire regime of solidification process into different sub-regimes, with contrasting rheological features. From a different viewpoint, Alexandrou et al. [8] have employed the single phase Herschel–Bulkley constitutive fluid model to simulate die filling. Such a model may be advantageous in a sense that it has the inherent capability to incorporate the finite yield stress and shear-thinning and thickening behavior that is typically displayed by semi-solid slurry. Kang et al. [9], however, have proceeded along the conventional approach of continuum formulation in order to treat the semi-solid slurry as a pseudo-Newtonian fluid at low solid fraction, by utilizing a semi-empirical treatment of viscosity in their mathematical model. Kotynia and Petera [10] have introduced a new general solidification model involving complex rheological properties of semi-solid metal alloys. They solved an additional momentum conservation equation to obtain liquid and solid phase velocities separately, and implemented the mathematical model in a finite element based algorithm. Chowdhury et al. [11], in a recent study, have developed an integrated continuum description of transport mechanisms characterizing the macrosegregation behavior in an electromagnetically stirred semi-solid material forming process. The authors, in their model [11], have considered the transport of fragmented solid phase and solidification of liquid phase through the solution of separate transport equations for liquid phase velocity and solid fraction evolution. However, there has been no attempt in their model to depict intricate momentum transport features through an improved and fundamental formulation of interphase interaction mechanisms and to relate the pertinent momentum exchanges with the corresponding rheological features. On the other hand, it can be well appreciated that the process of evolution of globular microstructure during semi-solid processing is strongly influenced by solid phase interactions, such as agglomeration and break-up. Unfortunately, to a large extent, such aspects have not been considered explicitly in any of the mathematical models on thermo-fluidic transport during SSM processing reported so far in the literature. In addition to this, the net rate of formation of aggregates also plays a crucial role in the determination of apparent viscosity. In reality, this fact could probably be taken care of only through the consideration of the evolution of a separate agglomeration parameter, which is yet to be invoked in the context of mathematical modeling of transport phenomena during SSM processing.

In this paper, an attempt has been made to develop a generalized and comprehensive approach for modeling transport phenomena during semi-solid materials processing, which takes into account the rheological aspects from a rather fundamental perspective, in comparison to other semi-empirical approaches commonly employed in the literature. In an effort to elaborate the pertinent rheological features from a fundamental viewpoint, physical situation of an electromagnetically stirred melt is simulated by employing two separate momentum transport models in the same unified framework. In the first model (Model A), local viscosity is assumed to be linearly linked with the solid fraction, whereas in the second model (Model

B), viscosity is assumed to be dependent on local strain rate as well as an agglomeration parameter that takes into account the solid phase interaction mechanisms. A quantitative comparison on the capabilities of individual models is also presented in details, so as to develop deeper insights into the implications of solid phase interaction mechanisms on the overall thermo-fluidic transport as well as the macrosegregation behavior.

2. Mathematical formulation

For convenience in description of the mathematical modelling approach, we consider the semi-solid processing of a binary alloy in a two-dimensional rectangular domain, in which the left boundary is subjected to prescribed temperature that is lower than the liquidus temperature corresponding to the initial alloy composition, whereas all other boundaries are kept insulated. The melt, with an initial superheat, is poured into the cavity, where it starts solidifying from the left vertical boundary. The problem domain is shown schematically in Fig. 1, describing the initial and boundary conditions. An electromagnetic stirrer is used for the generation of a rotating magnetic field. The electromagnetic stirring device consists of coils (through which the alternating current passes) wound around in a helical pattern [12]. In addition to this, the stirring system comprises of two transformers and a variable frequency drive. It is assumed that the frequency of alternating current field is high enough, in comparison to typical time steps used for numerical simulation, so that a time-averaged strength of magnetic field can be assumed, which simplifies the electromagnetic forces to functions of space co-ordinates alone. Basic features of typical electromagnetic stirrers can be found in the literature [12,13], and are omitted here for the purpose of brevity. It is noteworthy to mention here that the orientation of electromagnetic stirrer is taken to be such that electromagnetic force fields are dominant in the vertical plane only.

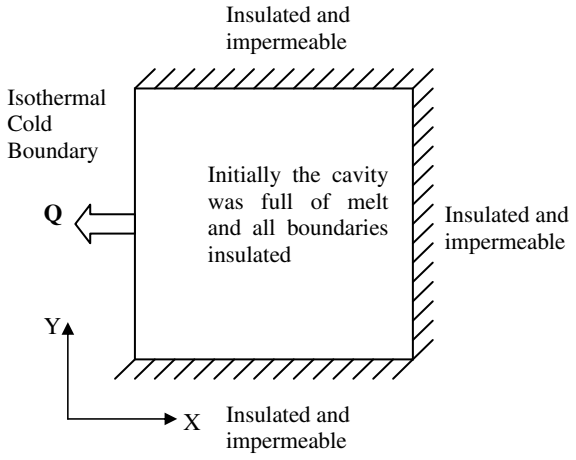

Fig. 1. The computational domain with pertinent initial and boundary conditions.

A general form of the governing differential equations pertinent to the above-mentioned physical situation, depicting the coupled transient transport of momentum, heat and solute, can be derived on the basis of a volume-averaged continuum approach [1], in which the details of micro and meso scale phenomena can be embedded through formulation of additional transport equations, coupled with thermodynamically consistent postulation of phase-change behavior. All the governing transport equations pertinent to an individual phase 'k', in the most general form, can be written in a generic form as

$$\frac{\partial}{\partial t}(\rho_k g_k \phi_k) + \nabla.(\rho_k g_k \phi_k \mathbf{V}_k) = \nabla.(g_k \Gamma_k \nabla \phi_k) + g_k S_k \qquad (1)$$

where ρ_k, g_k, Γ_k, $\mathbf{V}_k$ the density, volume fraction, diffusion coefficient of phase k and velocity vector respectively, ϕ_k is a general transport variable for phase k and S_k is the source term arising due to phase interaction. A subsequent summation of the individual phase equations would eventually lead to equivalent single phase transport equations, valid over the entire continuum domain. It can be noted here that specific forms of the governing transport equations depend on the manner in which inter phase interaction terms are mathematically handled. As mentioned earlier, here we aim to discuss on formalisms corresponding to two different physical models (to be described as 'model A' and 'model B' from here onwards) in the same generalized framework, so as to obtain deeper insights into their respective implications on the overall transport pattern. Basic contrasting features of the two models, in essence, are as follows:

1. *Model A*: This model entirely neglects the solid phase interaction mechanisms, and the solid phase transport is treated as a phenomenon having no impact on the apparent viscosity. In other words, the apparent viscosity variation is solely attributable to changes in local solid fraction.
2. *Model B*: In this model, a mesoscopic description is followed in which solid phase interactions are taken into account. For that purpose, an internal variable, namely, the agglomeration parameter is introduced and its evolution equation is solved to estimate the extent of solid phase interactions. The viscosity is treated as a function of the agglomeration parameter, local strain rate and local solid fraction.

It needs to be mentioned here that only the momentum conservation equations and the associated transport features differ for the two models, all other conservation equations virtually remaining the same. Table 1 depicts a generalized framework in which all the governing transport equations can effectively be cast, corresponding to both models A and B. Since, the solid particles within a semi-solid slurry remains fully dispersed in the liquid melt, an infinite diffusion of solute (on a local microscopic scale) in both solid and liquid phases may be assumed. Accord-

Table 1
General framework of the governing equations

Conservation of mass	$\frac{\partial}{\partial t}(\rho)+\nabla\cdot(\rho\mathbf{V})=0$ where $\rho=\sum_k\rho_k g_k$ and $\mathbf{V}=\sum\mathbf{V}_k f_k$
Conservation of momentum	$\frac{\partial(\rho\mathbf{V})}{\partial t}+\nabla\cdot(\rho\mathbf{V}\cdot\mathbf{V})=-\nabla p+\nabla\cdot(\mu_{\text{eff}}\nabla\mathbf{V})+\text{source terms}$
Conservation of thermal energy	$\frac{\partial(\rho h)}{\partial t}+\nabla\cdot(\rho\mathbf{V}h)=\nabla\cdot\left(\frac{k_{\text{eff}}}{C_p}\nabla h\right)+\text{source terms}$
Conservation of species	$\frac{\partial(\rho C_{\text{mix}})}{\partial t}+\nabla\cdot(\rho\mathbf{V}C_{\text{mix}})=\nabla\cdot\left(\frac{k_{\text{eff}}}{C_p}\nabla C_{\text{mix}}\right)+\text{source terms}$

ingly, the concentration in solid and liquid in a representative elemental microscopic volume can be considered as uniform, and therefore, the well-known Lever rule becomes applicable for modeling the microsegregation [14] features. In the present study, we do not attempt to present a detailed derivation of all the governing transport equations, and merely present the pertinent details in a tabular form (refer to Tables 2 and 3). Rather we focus on the contrasting features of momentum transport for the two models, which is the central theme of the present research.

Table 3
Supplementary relationships

Mixture composition definition	$C_{\text{mix}}=f_l C_l+f_S C_S$
Solid fragment transport equation	$\frac{\partial f_S}{\partial t}+\nabla\cdot(f_S\mathbf{V}_S)=\frac{\mathrm{d}f_S}{\mathrm{d}T}\frac{DT}{Dt}$
Liquid transport equation	$\rho_l f_l\frac{D\mathbf{V}_l}{Dt}=-f_l\nabla p+\nabla(f_l\underline{\underline{S}}_l)+\nabla(f_l\lambda_l\nabla\cdot\mathbf{V}_l)+\rho_l f_l\mathbf{g}+\mathbf{q}$ where $\underline{\underline{S}}$ is the stress tensor, $\mathbf{q}$ interaction force and λ_l is a constant dependent on Poisson's ratio

3. Details of momentum conservation formulation for the two models

3.1. Formulation for model A

In this model, the solid phase is assumed to be fully dispersed in the liquid melt. Under these circumstances, the solid phase may be considered as a pseudo-fluid with an enhanced viscosity. It is also worth mentioning here that model A is essentially similar to standard volume-averaged equivalent single phase models, often employed for phase change modeling in materials processing [1], and therefore all the details of the derivation will not be elaborated here. The set of momentum conservation equations for this model can be closed, based on an appropriate mathematical description of temperature, concentration, electromagnetic field (refer to Table 2 for mathematical description of pertinent source terms in the corresponding governing differential equations), as well as respective phase fractions, in conjunction with supplementary thermodynamic relationships (phase diagram information), macrosegregation model information as well as a description of liquid phase velocity (refer to Table 3 for details).

3.2. Formulation for model B

In this model, the physical situations prevailing in an electromagnetically stirred melt are accounted for, in a more fundamental manner. In contrast to model A, this

Table 2
Details of equivalent diffusion coefficients and source terms for the two models

Parameter	Model A	Model B
Viscosity	$\mu_{\text{eff}}=\mu_l g_l+\mu_s g_s$	$\mu_{\text{eff}}=(\eta_o+ksm\dot{\gamma}^{m-1})$
Thermal diffusion coefficient	$\Gamma=\frac{k_s'}{c_{ps}}f_s+\frac{k_l'}{c_{pl}}f_l$	Same as model A
Mass diffusivity	$\rho f_s D_S k_p+\rho f_l D_l$	Same as model A
Source terms in x-momentum equation	$-\nabla\cdot\left[\left(\mu_l\frac{\rho}{\rho_l}-\mu_s\frac{\rho}{\rho_s}\right)\nabla f_s u_s\right]-\nabla\cdot(\rho f_l f_s u_r\mathbf{V}_r)+(\mathbf{J}\times\mathbf{B})_x$	$\frac{1}{2}(\eta_o+ksm\dot{\gamma}^{m-1})\left(\frac{\partial^2 v}{\partial y\partial x}-\frac{\partial^2 u}{\partial y^2}\right)\frac{\partial}{\partial y}(\tau_y s)+\frac{\partial}{\partial x}(\tau_y s)+\dot{\gamma}_{xy}^m\frac{\partial(ks)}{\partial y}+\dot{\gamma}_{xx}^m\frac{\partial(ks)}{\partial x}-\nabla\cdot(\rho f_l f_s u_r\vec{V}_r)+(\mathbf{J}\times\mathbf{B})_x$
Source terms in y-momentum equation	$-\nabla\cdot\left[\left(\mu_l\frac{\rho}{\rho_l}-\mu_s\frac{\rho}{\rho_s}\right)\nabla f_s v_s\right]-\nabla\cdot(\rho f_l f_s v_r\mathbf{V}_r)+(\mathbf{J}\times\mathbf{B})_y+\rho[\beta_t(T-T_{\text{ref}})+\beta_s(C-C_{\text{ref}})]g$	$\frac{1}{2}(\eta_o+ksm\dot{\gamma}^{m-1})\frac{\partial}{\partial y}\left(\frac{\partial u}{\partial y}-\frac{\partial v}{\partial x}\right)\frac{\partial}{\partial y}(\tau_y s)+\frac{\partial}{\partial x}(\tau_y s)+\dot{\gamma}_{yy}^m\frac{\partial(ks)}{\partial y}+\dot{\gamma}_{xy}^m\frac{\partial(ks)}{\partial y}+\dot{\gamma}_{xx}^m\frac{\partial(ks)}{\partial x}-\nabla\cdot(\rho f_l f_s v_r\vec{V}_r)+\rho[\beta_t(T-T_{\text{ref}})+\beta_s(C-C_{\text{ref}})]g+(\mathbf{J}\times\mathbf{B})_y$
Source terms in energy equation	$-\frac{1}{C_p}\left\{\begin{array}{l}\nabla\cdot[\rho f_s(\mathbf{V}-\mathbf{V}_s)\Delta H]\\ -\frac{\partial}{\partial t}(\rho f_l\Delta H)-\nabla\cdot(\rho\mathbf{V}\Delta H)\end{array}\right\}$	Same as model A
Source terms in species conservation equation	$-\nabla\cdot[\rho f_s\mathbf{V}_s C_l(k_p-1)]-\frac{\partial}{\partial t}[\rho f_s C_l(k_p-1)]$	Same as model A

model attempts to address certain aspects of solid phase interactions, which have virtually been overlooked in the literature on multi-phase transport modeling. In particular, model B, in essence, also aims to incorporate rheological characteristics such as pseudoplasticity and thixotropy through inter-particle interaction mechanisms, and attempts a subsequent linking of the same with the pertinent momentum transport equations. This necessitates the introduction of an internal variable [15], in order to represent the state of agglomeration. In the internal variable framework, the interaction of particles is taken care of by assuming that the solid particles are rigid, forming an interconnected network as solidification progresses. This, in turn, ensures that solid velocity asymptotically tends to zero as more and more solid particles are agglomerated. This is in sharp contrast with model A, in which the solid velocities are insensitive to agglomeration between particles. This physical feature is effectively incorporated in model B by first appreciating that during intense stirring (mechanical or electromagnetic), the probability of interaction between two particles suspended in the melt increases by a large extent, so that certain phenomena like agglomeration and break-up play vital roles in significantly altering the transport behavior of melt. The macroscopic quantity through which such mesoscopic interactions are manifested most is the effective viscosity. Goutham and Kapur [16], in a different context, have proposed such a model in which they have considered the degree of agglomeration as an internal variable and solved an evolution equation of the agglomeration parameter. In this work, we aim to follow a similar approach. First, we note that if the semi-solid slurry is assumed to obey the Herschel–Bulkley constitutive model [8], the following form of relationship between stress, strain rate and agglomeration parameter can be used:

$$\tau(t) = (\tau_o + k\dot{\gamma}^m)s(t) + \eta_o\dot{\gamma} \tag{2}$$

where τ_o is shear yield stress of the suspension considered to be the Herschel–Bulkley fluid, $\dot{\gamma}$ is the local strain rate, m is the power law index, and k is the consistency coefficient. The parameters τ_o and k pertain to fully agglomerated state. The parameter η_o can be evaluated from the Krieger–Dougherty equation [16] for rigid spheres. Substituting Eq. (2) into the equation of motion, one can derive the following form of mixture momentum conservation equation in the x-coordinate direction:

$$\begin{aligned}\rho\frac{Du}{Dt} = &-\frac{\partial p}{\partial x} + (\eta_o + ksm\dot{\gamma}^{m-1})\nabla^2 u + \frac{1}{2}(\eta_o + ksm\dot{\gamma}^{m-1}) \\ &\times\left(\frac{\partial^2 v}{\partial y\partial x} - \frac{\partial^2 u}{\partial y^2}\right) + \frac{\partial}{\partial y}(\tau_o s) + \frac{\partial}{\partial x}(\tau_o s) + \dot{\gamma}_{xy}^m\frac{\partial(ks)}{\partial y} + \dot{\gamma}_{xx}^m\frac{\partial(ks)}{\partial x} \\ &- \nabla\cdot(\rho f_l f_s u_r\vec{V}_r) + (\mathbf{J}\times\mathbf{B})_x\end{aligned} \tag{3}$$

where f_l denotes the liquid mass fraction, f_s denotes the solid mass fraction, u_r denotes the relative velocity component along the x-direction and V_r is the relative velocity vector. $(\mathbf{J}\times\mathbf{B})_x$ represents component of electromagnetic force along x direction [12]. A similar approach can be followed for the y-momentum equation, as well. Regarding pertinent boundary conditions, it can be mentioned here that there can be an 'effective slip' between the solid particles and the mold wall, typically if the diameter of a solid particle adjacent to the wall is larger than the surface roughness length scale. However, in the literature, any kind of the experimental data correlating surface roughness with slip velocity, applicable to the physical situation presently under consideration, is not available. To resolve this situation, a model proposed by Ding and Gidaspow [17] may be adopted. According to that model, the tangential component of solid velocity at the wall is given as

$$(\mathbf{V}_s)_t|_w = -\lambda_p\left.\frac{\partial(\mathbf{V}_s)_t}{\partial n}\right|_w \tag{4}$$

where λ_p is the mean distance between particles, and is given by $\lambda_p = \frac{d_e}{\varepsilon_g^{\frac{1}{3}}}$. In this expression, d_e and ε_g are grain diameter and grain fraction, respectively.

It can be appreciated at this point that the agglomeration parameter appearing in Eqs. (2) and (3) need to be well-posed, in consistency with inter-particle interaction mechanisms. This can be achieved by invoking the following evolution equation for the agglomeration parameter [16]:

$$\frac{ds(t)}{dt} = -\bar{k}_b\dot{\gamma}s(t) + \frac{r_o + k_r'\dot{\gamma}}{1 + k_r''\dot{\gamma}^\varsigma}(1 - s(t))^2 \tag{5}$$

where $\varsigma, r_o, k_r\prime, k_r'', \bar{k}_b$ are functions of solid volume fraction, particle size and their respective distribution. In Eq. (5), the first term in RHS represents the effect of break-up on agglomeration, whereas the second term accounts for a reformation of the agglomerates. Necessary values of the model parameters can be obtained by referring to the work of Goutham and Kapur [16].

The solid velocity, as obtained from the above particle-based momentum transport model, needs to be adapted in accordance with the agglomeration parameter, for an effective prediction of the local momentum transport rates. In this context, earlier efforts have been based on certain empirical propositions, leading to switching off the solid phase velocity beyond an arbitrary critical value of solid fraction [18], which, by no means, follow from any theoretically derived formalism. In other words, such empirical considerations may turn out to be somewhat case-specific in nature. To avoid such empiricism, here we propose a fundamental micro-scale physics based approach for updating/modifying of the solid phase velocities, based on prevailing strain rates. This is systematically achieved as follows. First, we note that the shear force required for a break-up of solid particles into clusters can be described as: $F_s = \frac{\pi}{4}D^2\mu\dot{\gamma}$, where $\dot{\gamma}$ is the shear strain rate and D is the cluster diameter. On the other hand, agglomeration between particles is aided by the corresponding Vander-Wall's force of attraction, which can be modeled

as follows. First, a Vander-Wall's force of attraction between two equal sized particles is given as: $F_a = \frac{Ad_p^o}{24H^2}$, where A is the Hamaker's constant and H is the closest distance between surface of adjacent particles. Next, we consider a cluster of such particles. For instance, if a cluster contains N particles of diameter d_p^o with a volume fraction of α_p, the cluster diameter is given as: $D = \left(\frac{N}{\alpha_p}\right)^{1/3} d_p^o$. Accordingly, the number concentration of elementary particles becomes: $n = \frac{N}{\frac{\pi}{6}D^3}$. If we assume that the volume of elementary particles containing contact points to be $V^* = \frac{\pi}{4}D^2 d_p^o$, then the number of contact points along the cluster split surface is given by: $N_c = nV^*$. Hence, for the cluster, after assemblage, the containing force becomes: $F_v = N_c.F_a = \frac{\alpha_p}{16}\left(\frac{N}{\alpha_p}\right)^{1/3}\frac{Ad_p^o}{H^2}$. On the other hand, the net shear induced disruptive force is given as: $F_s = \mu\dot{\gamma}\left(\frac{N}{\alpha_p}\right)^{2/3}\frac{\pi}{4}d_p^{o2}$. In practice, N may be assumed to be a linear function of agglomeration parameter (with a maximum value equal to the grain density), and α_p can be taken as the maximum solid fraction which can occur in a close-packed cluster of spherical particles. When local strain rates are such that the shear force is greater than the containing force, a break-up may occur, whereas a greater containing force would eventually lead to agglomeration. Consequently, the condition for break-up (i.e., $F_s \geqslant F_v$) gives rise to a critical rate of shear strain, beyond which agglomeration of particles may not be possible. Utilizing this criterion, one may obtain a ratio $r = N_a/N_t$, where N_a is the total number of control volumes in which agglomeration is predicted to occur, out of N_t number of control volumes present in the computational domain in totality. The parameter r, hence, can be described as a measure of the extent of agglomeration, and the solid velocity would be theoretically zero if r equals unity. Hence, the solid velocity obtained from solution of momentum conservation equations can be corrected by multiplying with a factor of $(1 - r)$ such that $v_s = 0$ when $r = 1$.

4. Numerical implementation

The two different transport models described here are utilized to simulate the continuous solidification process of a binary Pb–Sn (lead–tin) metal alloy subjected to an electromagnetic stirring action in a 0.1 m × 0.1 m rectangular cavity. The relevant problem data are presented in Table 4. The governing transport equations are discretized by employing a finite volume scheme [19]. For the purpose of pressure-velocity coupling, the SIMPLER algorithm [19] is followed. At the beginning of the numerical procedure, velocity, temperature and concentration values are evaluated on the basis of an assumed solid velocity field. The liquid phase velocities are obtained from the pertinent transport equation, and hence the solid phase velocity is recalculated by utilizing the expression of continuum velocity in terms of respective constituent phase velocities. For model B, this is corrected by multiplying with a factor of $(1 - r)$. This procedure is iterated within a particular time-step, till a final convergence in all the field variables is achieved. Further, for accurate prediction of the liquid fraction in the present 'fixed-grid enthalpy-based' procedure, the latent enthalpy of each computational cell is updated according to the temperature and/or species concentration values predicted by the macroscopic conservation equations, during each iteration within a time-step [14]. In a physical sense, such updating attempts to neutralize the difference in the nodal temperature predicted from the energy equation, and that dictated by the phase-change considerations. Convergence is declared, when, during the inner iterations in each time step, relative errors in the magnitude of velocity, energy and concentration values fall below a certain predetermined limit ($<10^{-3}$%). Different grid sizes (42×42, 62×62 and 102×102) are employed for the resolution of computational domain of size (0.1 m × 0.1 m) to check for grid independence. In a computational platform based on Pentium® 4 processor and 2 GB RAM, numerical simulation of 0.1 s of real time takes about 13.5 CPU-s for model A, while 16.3 CPU-s are taken for model B.

Table 4
Thermophysical properties and problem data

Parameter	Value
Thermal conductivity of liquid	30 W m^{-1} K^{-1}
Thermal conductivity of solid	60 W m^{-1} K^{-1}
Specific heat for both liquid and solid	154.6 J kg^{-1} K^{-1}
Initial temperature	623.16 K
Cold wall temperature	423.16 K
Solutal volumetric expansion coefficient	−0.113
Electrical conductivity of the alloy	9.09×10^6 Ω^{-1} m^{-1}
Density of solid	10100 kg m^{-3}
Apparent viscosity of solid	1.85×10^4 kg m^{-1} s^{-1}
Apparent viscosity of liquid	2.53×10^{-3} kg m^{-1} s^{-1}
Thermal volumetric expansion coefficient	1.2×10^{-4} K^{-1}

5. Results and discussion

Fig. 2 shows the electromagnetic force distribution in the melt generated by electromagnetic stirring. The nature

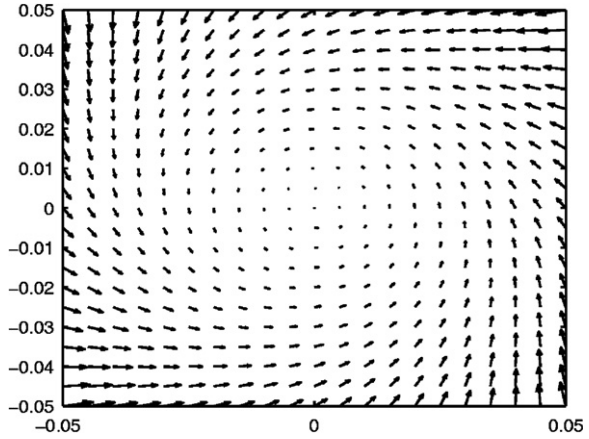

Fig. 2. Distribution of electromagnetic force generated by a rotary magnetic field.

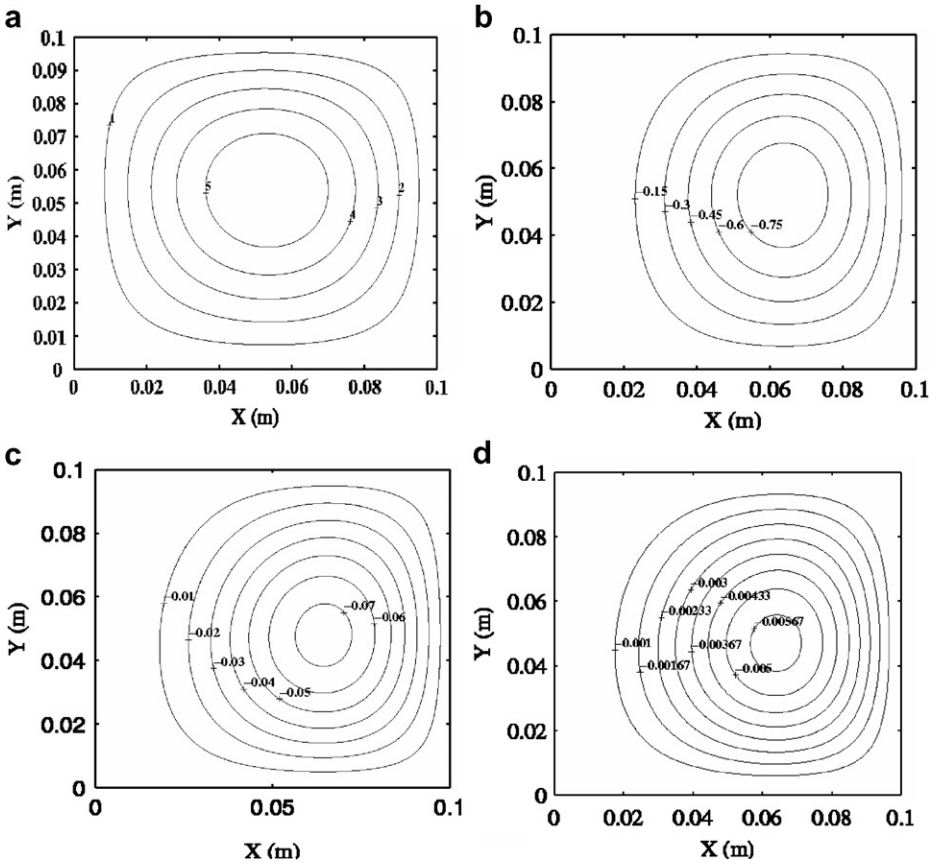

Fig. 3. Streamlines corresponding to model A, at different stages of solidification. (a) $t = 50$ s, (b) $t = 100$ s, (c) $t = 200$ s and (d) $t = 300$ s.

of the electromagnetic forces clearly illustrates the generation of a magnetic field with a rotating vector. Fig. 3 depicts the streamline patterns obtained by employing model A, at different instants of time. The streamlines apparently portray a generalized flow pattern, as a consequence of an electromagnetically stirred field. The major vortices, as observed in the convection patterns, can clearly be attributed to the effects of these electromagnetic stirring forces. However, as solidification progresses, the net momentum transfer significantly weakens. From physical nature of the transport processes, it is expected that an enhanced interaction between solid particles, owing to the intense stirring, is also likely to increase the overall resistance against momentum transfer [12,13]. Model B captures this behaviour in a more realistic fashion, by taking care of solid phase interaction mechanisms, leading to a quicker decay in the velocity field. Moreover, at later stages of solidification, local islands of solid phase may form, which remain interconnected in a network. As a result, the length scale of momentum transport is likely to get reduced, and locally constrained flows may be observed. The above formation of interconnected network, further, would not allow the solid phase to move appreciably, and the effects of liquid stirring would eventually turn out to be somewhat localized. The liquid velocity, in these circumstances, would be primarily affected by thermosolutal buoyancy effects, and less prominently by electromagnetic forces. This is also tested in the numerical simulation by switching 'on' and 'off' the respective electromagnetic force terms towards the later transients. Essentially, the similar nature of convection patterns are obtained in both the cases, thereby demonstrating the fact the convection patterns are dominated by the thermosolutal buoyancy effects towards the later stages of solidification. Referring to streamline patterns at $t = 200$ s for model B (Fig. 4), locally recirculating motions can be observed at considerable distance from the cold wall, which may be attributed to local double-diffusive effects. Model A does not account for such solid phase interactions and, therefore is incapable of predicting the concerned localized flow behaviour. Such limitations are eliminated from Model B, with the introduction of an additional equation of state variable, leading to an effective capturing of local recirculatory flows, especially at later instants of time.

Although the energy and species transport are governed by same form of equations in both the models, it is the change in the momentum transfer model which results in the difference in natures in isotherms and isoconcentration lines for the two models. Isotherms at different instants of time, for model A (refer to Fig. 5), exhibit that the dominant mode of heat transfer gradually transits from advection to conduction, with an increased presence of solid

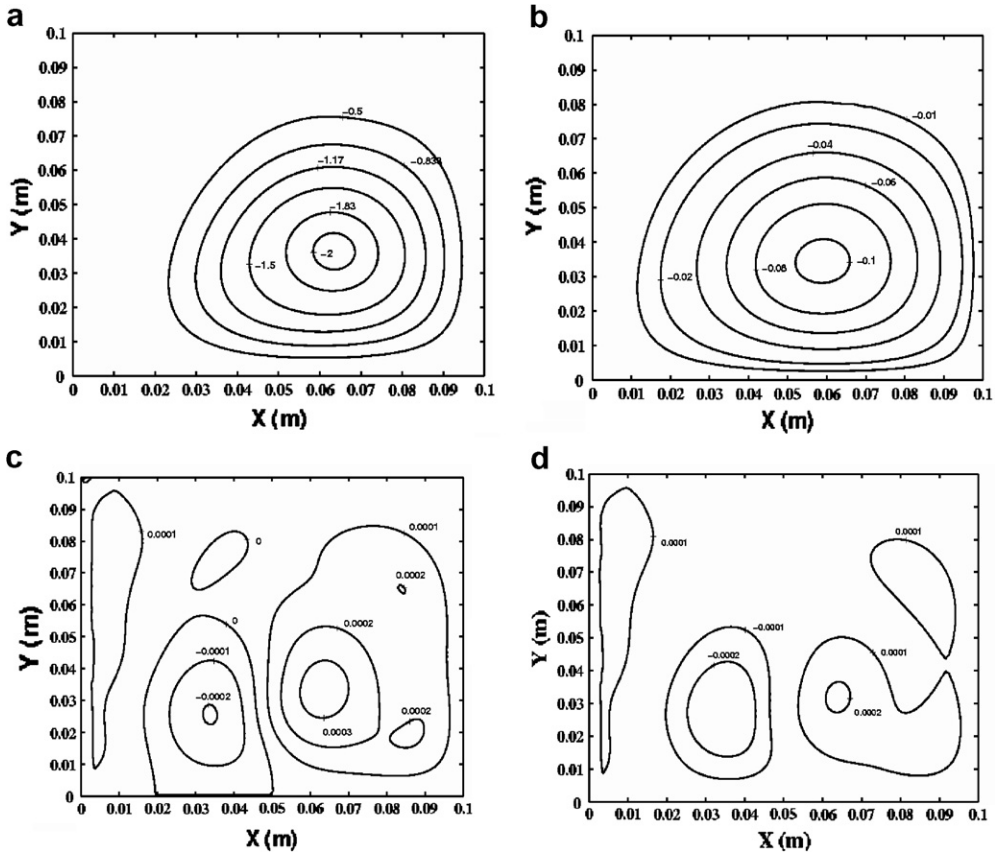

Fig. 4. Streamlines corresponding to model B, at different stages of solidification. (a) $t = 50$ s, (b) $t = 100$ s, (c) $t = 200$ s and (d) $t = 300$ s.

phase in the domain. However, in this context, it can be noted that model A overestimates advection transport at later stages of solidification, due to its inherent inability in capturing solid phase interactions. Hence, even at later stages of solidification (when mixture velocity virtually ceases to exist), isotherms for model A exhibit characteristic curvatures that are otherwise indicative of a strong advective transport. Model B, however, does not suffer from such limitations (refer to isotherms depicted in Fig. 6). Additionally, model B effectively captures the formation of aggregates. This, in turn, promotes conduction heat transfer in the intermediate stages, which is a natural outcome of an increased level of overlapping between solid phases and an enhanced interaction between solid particles due to agglomeration. Such enhancements in effective conduction during evolution of the solidification process cannot be predicted by model A.

The concentration patterns exhibited by the two models may also be reviewed to highlight their relative differences in terms of respective quantitative capabilities in predicting the macrosegregation behaviour. Fragments which form at the initial stages of solidification are advected away from the cold wall, primarily due to an intense stirring caused by the electromagnetic force. These fragments get deposited in a region near the walls, where the velocity is rather low. This leads to low concentration zones in vicinity of the walls, which is featured in predictions from both models A and B (refer to Figs. 7 and 8). However, model A is unable to predict any local fluctuations in concentration occurring due to the remelting of advected chunks of solid. Such advection of large chunks of solid phase, formed due to agglomeration, plays a significant role in the determination of the macrosegregation, in practice. In fact, it is highly probable that solid chunks formed at early stages of solidification, containing a small amount of entrained melt, may be able to maintain their existence. This, aided by solid phase advection, can result in local concentration fluctuations. This is observed in the snapshot of mixture concentration taken at $t = 50$ s, as depicted in Fig. 8. However, at later stages of solidification (when overall solid content becomes high and the mixture velocity becomes very low), the advection of solid chunks become a distant possibility, and the mixture concentration profile get virtually free from characteristic local fluctuations.

For an overall assessment of the predictions of the two models, following aspects may carefully be noted. During the initial stages of solidification, the overall melt temperature remains considerably high and the size of solid particles is not high enough to form large aggregates by the process of agglomeration. As a result, the transport phenomena are more or less accurately accounted for by the model A, and no discrepancy arises between expected

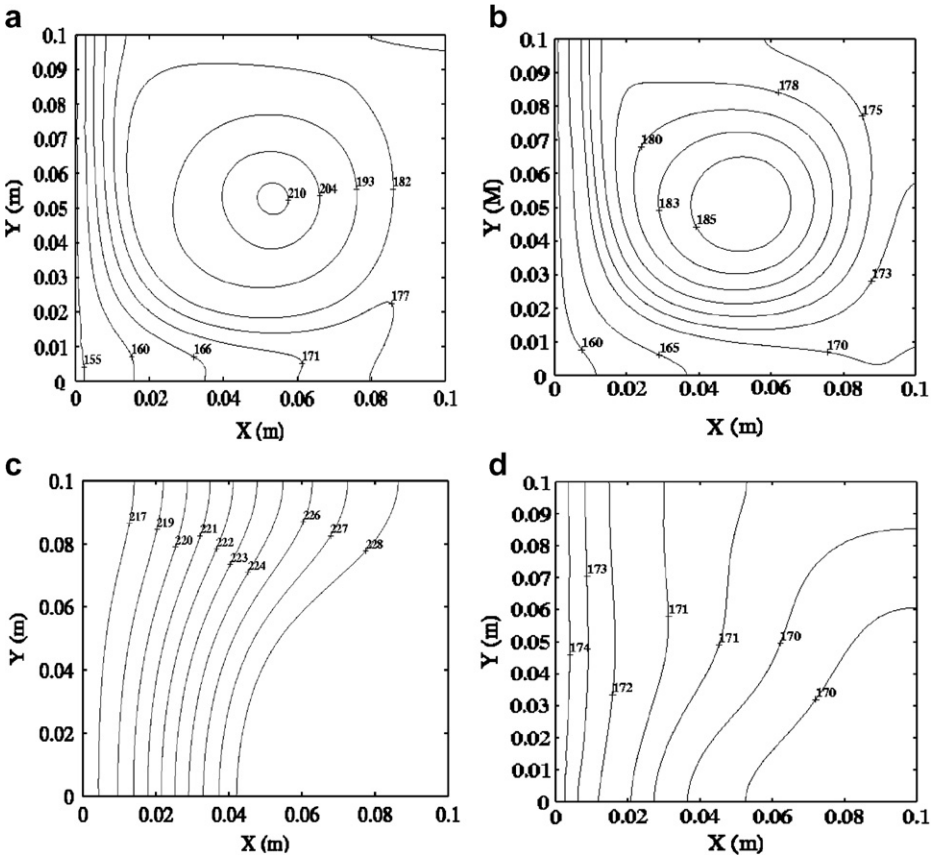

Fig. 5. Isotherms corresponding to model A, at different stages of solidification. (a) $t = 50$ s, (b) $t = 100$ s, (c) $t = 200$ s and (d) $t = 300$ s.

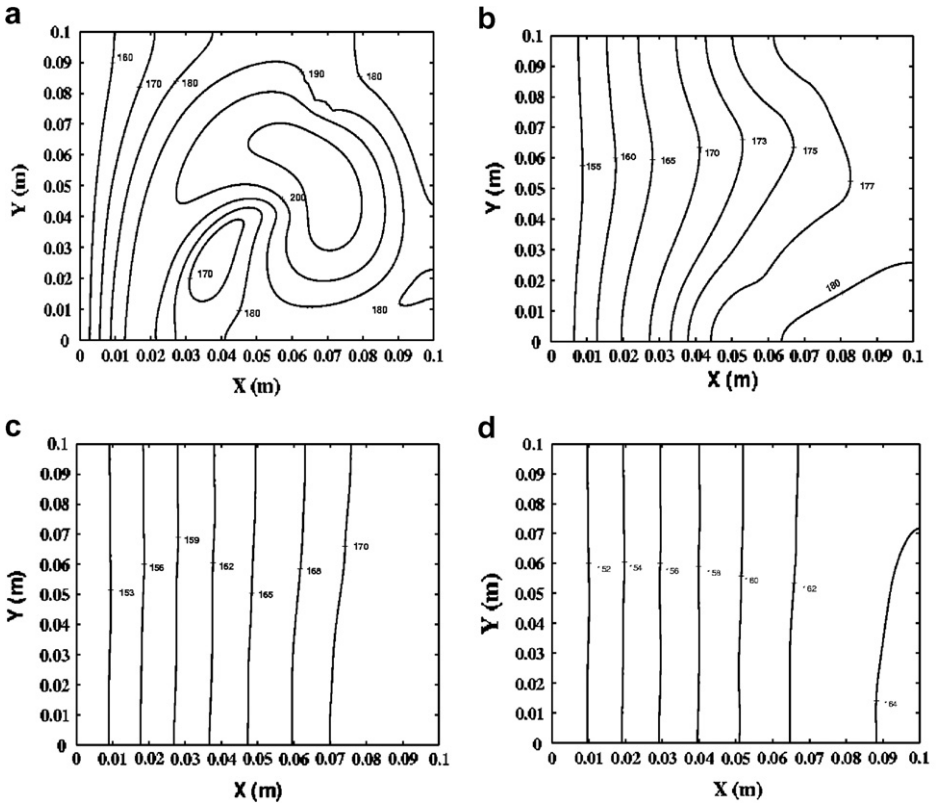

Fig. 6. Isotherms corresponding to model B, at different stages of solidification. (a) $t = 50$ s, (b) $t = 100$ s, (c) $t = 200$ s and (d) $t = 300$ s.

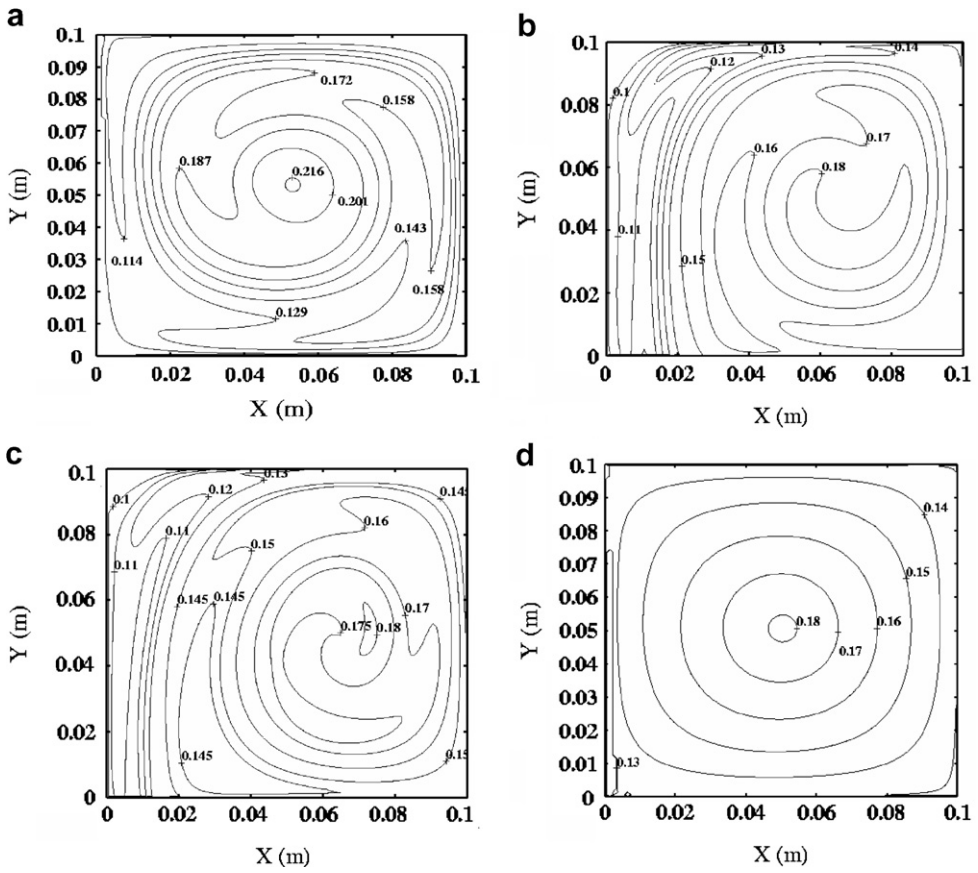

Fig. 7. Iso-concentration lines corresponding to model A, at different stages of solidification. (a) $t = 50$ s, (b) $t = 100$ s, (c) $t = 200$ s and (d) $t = 300$ s.

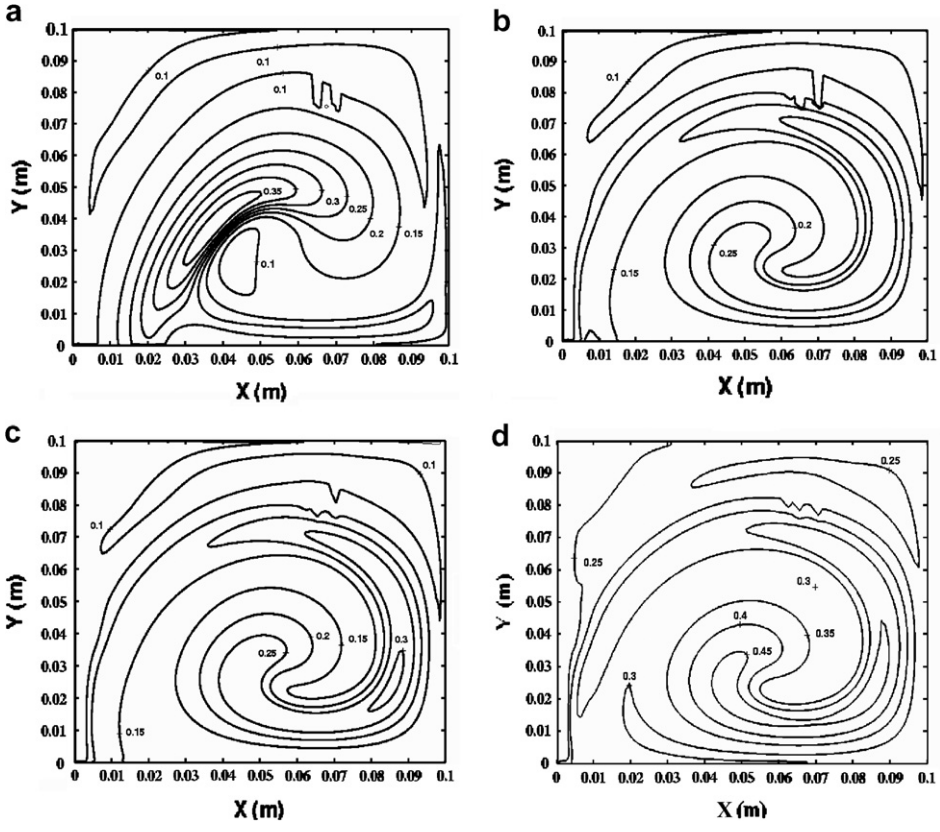

Fig. 8. Iso-concentration lines corresponding to model B, at different stages of solidification. (a) $t = 50$ s, (b) $t = 100$ s, (c) $t = 200$ s and (d) $t = 300$ s.

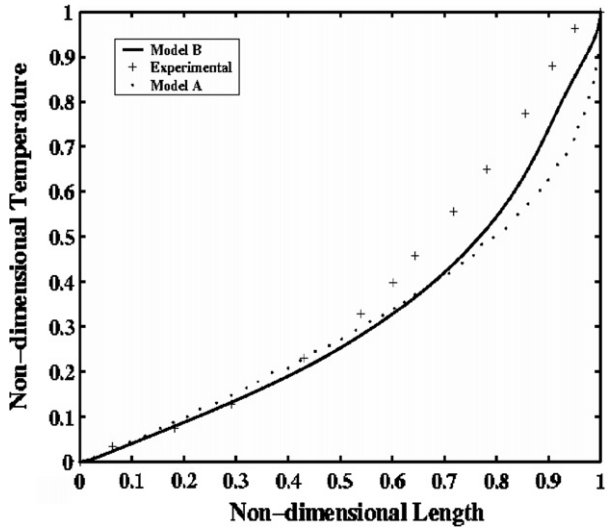

Fig. 9. Comparison with experiments [20], corresponding to axial distribution of temperature at $t = 120$ s, for both models.

physical behaviour and results from the numerical simulation. However, at later stages of solidification, the overall solid fraction becomes substantial to promote the formation of large aggregates, leading to an enhanced interaction between solid particles. Model A turns out to be insufficient to capture these interactions. On the other hand, Model B follows a more rigorous approach in terms of predicting local viscosity variations, based on internal variables and kinetic evolution of an agglomeration parameter. Also, the solid velocity is extinguished gradually by taking care of relative contributions of attractive forces and shear forces in the formation of an interconnected network. In model B, the momentum transfer is accordingly dictated by evolution of the internal variable and local strain rates. Evidently this can be justified as a more efficient way of modeling zones with high velocity gradients near the interconnected solid network.

6. Comparison with experiments

In order to assess the relative performance of the two models in practical situations, experimental results obtained by Roplekar and Dantzig [20] are utilized. The above experiments have been conducted for solidification in a cavity cooled from bottom, with an initial superheat and in the presence of a rotational magnetic field. A detailed scrutiny of the axial temperature profiles, as depicted in Fig. 9, reveals that a negligible difference in predictions of the two models can be observed near the cold wall, where solid fraction is very high. However, at a considerable distance from the cold wall, interaction of agglomerated solid phases with the surrounding fluid turns out to be a key mechanism dictating the overall transport, which cannot be captured by model A. This is emphasized out by the fact that predictions from Model B (refer to Fig. 9) are more close to the experimental results. This establishes the superiority of the model B in simulating SSM processing, as compared to the other existing models.

7. Conclusions

In this work, rheological aspects of a stirred semi-solid slurry have been explored, through a comparative study of two theoretical approaches, distinguished by two contrasting traits of simplicity and accuracy. The first approach, which is based on the assumption of a fully dispersed solid in liquid melt, has been found to be adequate in predicting gross transport characteristics through a solution of the pertinent conservation parameters. However, the second approach, based on an agglomeration parameter based internal variable postulate, more efficiently captures the solid phase interactions, and hence overshadows the first model from considerations of accuracy and efficient resolution of intricate transport features in semi-solid slurry processing. Only drawback lying with this approach is the increased computational cost that one needs to pay for solution of additional evolution equations. Once such restrictions are overcome to some extent, future researches may concentrate on an extension of the present theoretical approach to predict shape and size of solidified crystals in semi-solid materials processing, through an appropriate and efficient macro–micro coupling.

References

[1] W.D. Bennon, F.P. Incropera, A continuum model for momentum, heat and species transport in binary solid–liquid phase-change systems-I. Model formulation, Int. J. Heat Mass Transfer 30 (1987) 2161–2170.
[2] M.C. Flemings, Behavior of metal alloys in the semisolid state, Metall. Trans. A 22A (1991) 957–981.
[3] D.H. Kirkwood, Semisolid metal processing, Int. Mater. Rev. 39 (1994) 173–189.
[4] P. Kumar, C.L. Martin, S. Brown, Constitutive modeling and characterization of the flow behavior of semi-solid metal alloy slurries – I. The flow response, Acta Metall. Mater. 42 (1994) 3595–3602.
[5] C.L. Martin, P. Kumar, S. Brown, Constitutive modeling and characterization of the flow behavior of semi-solid metal alloy slurries – II. Structural evolution under shear deformation, Acta Metall. Mater. 42 (1994) 3603–3614.
[6] Z. Fan, Semisolid metal processing, Int. Mater. Rev. 47 (2002) 49–85.
[7] M.D. Mat, O. J Illegbusi, Application of a hybrid model of mushy zone to macrosegregation in alloy solidification, Int. J. Heat Mass Transfer 45 (2002) 279–289.
[8] A. Alexandrou, F. Berdinet, W. Loue, Mathematical and computational modeling of die filling in semisolid metal processing, J. Mater. Process Technol. 96 (1999) 59–72.
[9] C.G. Kang, J.S. Choi, D.W. Kang, A filling analysis of the forging process of semi-solid aluminum materials considering solidification phenoemena, J. Mater. Process Technol. 73 (1998) 289–302.
[10] J. Petera, M. Kotynia, The finite element model of non-isothermal semi-solid fluid flow, Int. J. Heat Mass Transfer 47 (2004) 1483–1498.
[11] J. Chowdhury, S. Ganguly, S. Chakraborty, Numerical simulation of transport phenomena in electromagnetically stirred semi-solid materials processing, J. Phys. D: Appl. Phys. 38 (2005) 2869–2880.

[12] J. Partinen, N. Saluja, J. Szekely, J. Kirtley, Experimental and computational investigation of rotary electromagnetic stirring in a woods metal system, ISIJ Int. 34 (1994) 707–714.
[13] H.K. Moffatt, Electromagnetic stirring, Phys. Fluids A 3 (1991) 1336–1343.
[14] V.R. Voller, A.D. Brent, C. Prakash, The modeling of heat, mass and solute transport in solidification systems, Int. J. Heat Mass Transfer 32 (1989) 1719–1731.
[15] P. Kumar, Constitutive modeling and characterization of the flow behavior of semi-solid metal alloy slurries, Ph.D. thesis, MIT, 1994.
[16] B.P. Gautham, P.C. Kapur, Rheological model for short duration response of semi-solid metals, Mater. Sci. Eng. A 393 (2005) 223–228.
[17] J. Ding, D. Gidaspow, A bubbling fluidization model using kinetic theory of granular flow, AIChE J. 36 (1990) 523–538.
[18] D.B. Spencer, R. Mehrabian, M.C. Flemings, Theoretical behaviour of Sn–15 pct Pb in crystallization range, Metall. Trans. 3 (1972) 1925–1932.
[19] S.V. Patankar, Numerical Heat Transfer and Fluid Flow, Hemisphere Publishing Corporation, Washington, DC, 1980.
[20] J.K. Roplekar, J.A. Dantzig, A study of solidification with a rotating magnetic field, Int. J. Cast Met. Res. 14 (2001) 79–95.